How to cite: *Angew. Chem. Int. Ed.* **2023**, *62*, e202312610
doi.org/10.1002/anie.202312610

Graphene

$N=8$ Armchair Graphene Nanoribbons: Solution Synthesis and High Charge Carrier Mobility**

Xuelin Yao, Heng Zhang, Fanmiao Kong, Antoine Hinaut, Rémy Pawlak, Masanari Okuno, Robert Graf, Peter N. Horton, Simon J. Coles, Ernst Meyer, Lapo Bogani, Mischa Bonn, Hai I. Wang,* Klaus Müllen,* and Akimitsu Narita**

Abstract: Structurally defined graphene nanoribbons (GNRs) have emerged as promising candidates for nanoelectronic devices. Low band gap (<1 eV) GNRs are particularly important when considering the Schottky barrier in device performance. Here, we demonstrate the first solution synthesis of 8-AGNRs through a carefully designed arylated polynaphthalene precursor. The efficiency of the oxidative cyclodehydrogenation of the tailor-made polymer precursor into 8-AGNRs was validated by FT-IR, Raman, and UV/Vis-near-infrared (NIR) absorption spectroscopy, and further supported by the synthesis of naphtho[1,2,3,4-*ghi*]perylene derivatives (**1** and **2**) as subunits of **8-AGNR**, with a width of 0.86 nm as suggested by the X-ray single crystal analysis. Low-temperature scanning tunneling microscopy (STM) and solid-state NMR analyses provided further structural support for **8-AGNR**. The resulting **8-AGNR** exhibited a remarkable NIR absorption extending up to ~2400 nm, corresponding to an optical band gap as low as ~0.52 eV. Moreover, optical-pump TeraHertz-probe spectroscopy revealed charge-carrier mobility in the *dc* limit of ~270 $cm^2 V^{-1} s^{-1}$ for the **8-AGNR**.

Graphene nanoribbons (GNRs) are promising candidates for next-generation nanoelectronics with high charge-carrier mobilities and non-zero band gaps.[1] Bottom-up synthesis, typically through on-surface or solution-mediated protocols, has provided atomically precise GNRs with diverse edge structures,[2] revealing not only their structure-dependent electronic and optical properties, but also the emergence of exotic topological phases[3] and magnetic edge states.[4] While GNRs with zigzag edges are prone to be oxidized under air,[5] armchair GNRs (AGNRs) are promising for electronic device applications considering their high chemical stability and sizable band gaps that are tunable by tailoring their width.[6]

AGNRs can be divided into three subfamilies of $N=3p$, $N=3p+1$, and $N=3p+2$, where p is an integer and N denotes the rows of carbon atoms across the ribbon width.[6a] In recent years, AGNRs of the first two subfamilies have been extensively investigated, confirming the predicted semiconducting properties with large band gaps for $N=7$, 9, and 13.[7] On the other hand, AGNRs that fall into the $N=3p+2$ subfamily are expected to possess excellent electrical properties, arising from their predicted low carrier effective masses, which lead to higher charge-carrier

[*] Dr. X. Yao, Dr. H. Zhang, Dr. R. Graf, Prof. Dr. M. Bonn, Prof. Dr. H. I. Wang, Prof. Dr. K. Müllen, Prof. Dr. A. Narita
Max Planck Institute for Polymer Research
Ackermannweg10, 55128 Mainz (Germany)
E-mail: xuelin.yao@materials.ox.ac.uk
wanghai@mpip-mainz.mpg.de
muellen@mpip-mainz.mpg.de
akimitsu.narita@oist.jp

Dr. X. Yao, F. Kong, Prof. Dr. L. Bogani
Department of Materials
University of Oxford
OX13PH Oxford (United Kingdom)

Dr. A. Hinaut, Dr. R. Pawlak, Prof. Dr. E. Meyer
Department of Physics
University of Basel
Klingelbergstrasse 82, 4056 Basel (Switzerland)

Prof. Dr. M. Okuno
Department of Basic Science, Graduate School of Arts and Sciences
The University of Tokyo
3-8-1 Komaba, Meguro, 153-8902 Tokyo (Japan)

Dr. P. N. Horton, Prof. Dr. S. J. Coles
National Crystallography Service, School of Chemistry
University of Southampton
SO171BJ Southampton (United Kingdom)

Prof. Dr. H. I. Wang
Nanophotonics, Debye Institute for Nanomaterials Science
Utrecht University
Princetonplein 1, 3584CC, Utrecht (The Netherlands)

Prof. Dr. A. Narita
Organic and Carbon Nanomaterials Unit
Okinawa Institute of Science and Technology Graduate University
904-0495 Okinawa (Japan)

[**]A previous version of this manuscript has been deposited on a preprint server (https://doi.org/10.26434/chemrxiv-2023-bhmw3).

mobilities.[8] However, this subfamily of AGNRs has been relatively underexplored.

On-surface synthesis has successfully delivered 5-AGNRs,[9] the narrowest GNR of $N=3p+2$ subfamily, and a wider 17-AGNRs[10] with a small band gap of 0.19 eV using tailor-made precursors. In addition, the lateral fusion of 3- and 5-AGNRs provided 8-AGNR fragments, and 14-AGNRs were concomitantly formed during the growth of 7-AGNRs,[11] but their selective on-surface synthesis remains elusive.[12] Notably, Rubin et al. described the synthesis of 8-AGNRs through the solid-state Hopf pericyclic reaction of polydiacetylenes,[13] but the optical band gap of the obtained sample was not reported, presumably due to the insolubility. In comparison to the on-surface and solid-state synthesis methods that are constrained by limited processability of the resulting GNRs, solution-mediated synthesis can be an attractive alternative to enable the liquid-phase processing.[14] A solution synthesis of 5-AGNRs was reported by alkyne benzannulation,[15] and also attempted by cyclodehydrogenation of poly(perylene),[16] but the wavelengths of their optical absorption edges were much shorter than expected from the theoretically predicted band gap of 5-AGNRs.[6a] Moreover, the solution synthesis of wider AGNRs belonging to the $N=3p+2$ subfamily has remained challenging.

Herein we report the solution-synthesis of 8-AGNRs through the Scholl reaction of an arylated polynaphthalene precursor. The successful formation of 8-AGNRs was corroborated by Fourier-transform infrared (FT-IR) and Raman spectroscopy, solid-state NMR analyses, and scanning probe microscopy, as well as supported by the highly efficient synthesis of naphtho[1,2,3,4-*ghi*]perylene derivatives(**1** and **2**) as model compounds. Remarkably, the resulting 8-AGNRs revealed a near-infrared (NIR) absorption extending up to 2400 nm, corresponding to an optical band gap of as low as 0.52 eV in line with the theoretical prediction.[17] Besides, time-resolved TeraHertz (THz) spectroscopy demonstrated a high short-range charge-carrier mobility up to ~270 and ~170 $cm^2 V^{-1} s^{-1}$ in dispersion and the thin-film of **8-AGNR**, respectively, suggesting its great potential for applications in electronic devices.

The synthesis of naphtho[1,2,3,4-*ghi*]perylene derivatives (**1** and **2**) as model compounds is depicted in Scheme 1. 2-[4-(*tert*-Butyl)phenyl]-1,1′-binaphthyl (**5**) was first synthesized through bromination of 2-[4-(*tert*-butyl)phenyl]naphthalene (**3**) to give 1-bromo-2-[4-(*tert*-butyl)phenyl]naphthalene (**4**), followed by a Suzuki coupling with 1-naphthylboronic acid. The Scholl reaction of **5** with 2,3-dichloro-5,6-dicyano-1,4-benzoquinone (DDQ)/trifluoromethanesulfonic acid (TfOH) at 0 °C afforded **1** as a yellow solid in 33 % yield. The low yield of **1** could be ascribed to a competing dimerization of **1** during the Scholl reaction, as indicated by mass spectroscopy results (see Figure S1). A similar dimerization of triphenylene was reported under the Scholl reaction of unsubstituted *o*-terphenyl.[18] To circumvent this issue, we re-designed the model structure to compound **2**, introducing bulky substituents, i.e., mesityl groups, on the naphtho[1,2,3,4-*ghi*]perylene core. Toward the synthesis of 2-[4-(*tert*-butyl)phenyl]-4,4′-dimesityl-1,1′-binaphthalene (**11**) as the precursor of **2**, 1-bromo-3-iodonaphthalene (**6**) was initially prepared (see synthetic details in Supporting Information). Two aryl groups were then installed sequentially at the naphthalene core of **6** via selective Suzuki coupling, followed by bromination to give 1-bromo-2-[4-(*tert*-butyl)phenyl]-4- mesitylnaphthalene (**9**). Subsequently, Suzuki coupling of **9** with (4-mesitylnaphthalen-1-yl)boronic acid (**10**) provided **11** in 69 % yield. Cyclodehydrogenation of **11** with DDQ/TfOH furnished compound **2** in an excellent yield of 95 % and no dimerized product was detected by mass spectrometry (Figure S2).

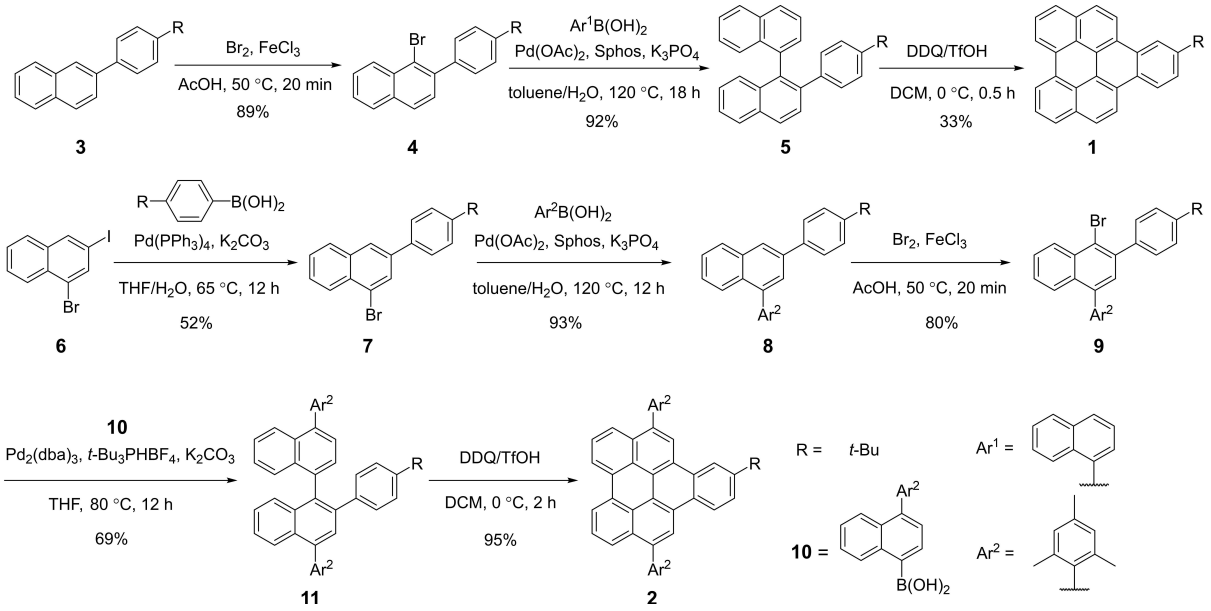

Scheme 1. Synthetic routes to compounds **1** and **2**.

Compounds **1** and **2** were initially characterized by matrix-assisted laser desorption/ionization time-of-flight mass spectrometry (MALDI–TOF MS), which displayed the expected molecular mass, and NMR spectroscopy showed well-resolved proton signals that could be fully assigned (see MALDI-TOF MS and NMR spectra in Supporting Information). Moreover, single crystals suitable for the X-ray diffraction analysis could be obtained by slow evaporation of their solutions in dichloromethane, unambiguously revealing their structures (Figure 1).[19] Compound **1** has a planar geometry while the aromatic core of **2** is slightly bent due to the mesityl groups. Both **1** and **2** adopt lamellar packing motifs, although the latter has a larger packing distance. Additionally, a width of 0.86 nm can be estimated for 8-AGNRs from the structure of **1** (Figure 1a).

Encouraged by the successful synthesis of model compound **2**, the synthetic route to 8-AGNRs was designed as illustrated in Scheme 2. First, dibromoarene **13** was synthesized by silver-mediated direct arylation of 1,4-dibromonaphthalene with 1-(4-decylhexadecyl)-4-iodobenzene (**12**).[20] Subsequently, selective monolithiation/borylation of **13** furnished arylated naphthalene isomers **14** and **14′** functionalized with bromo and boronic ester groups, which could be easily separated by silica gel column chromatography (see Supporting Information for details). Palladium-catalyzed AB-type Suzuki polymerization of **14** provided arylated polynaphthalene precursor **P1** with pendent branched alkyl chains. After the removal of short oligomers via recycling gel permeation chromatography (GPC), analysis of **P1** by size exclusion chromatography (SEC) against linear polystyrene standard indicated a number-average molecular weight (*M*n) of about 3.3×10^4 g mol^{-1} and a polydispersity index (PDI) of 2.0 (Figure S3). MALDI-TOF MS characterization revealed a regular pattern with peak-to-peak distance of ~567, corresponding to the molecular mass of the repeating unit (Figure S4). Finally, the Scholl reaction of **P1** with DDQ/TfOH in dichloromethane afforded **8-AGNR**. The estimated average length of **8-AGNR** is ~20 nm based on the SEC analysis of **P1**.

The successful transformation of **P1** into **8-AGNR** via the Scholl reaction was initially corroborated by FT-IR spectroscopic analyses combined with density functional theory (DFT) simulations (Figure 2a; see Supporting Information for the details of the simulation). Distinct C–H out-of-plane (*opla*) vibrational modes, defined as SOLO, DUO, and QUATRO, which are strongly associated with the number of adjacent C–H bonds (highlighted with different colors in Figure 2a),[21] provide a precise fingerprinting of the molecular structures. **P1** is characterized by the QUATRO mode at 761 cm^{-1} (olive-colored), which is significantly attenuated in the spectrum of **8-AGNR**, indicating the efficient cyclization of the polynaphthalene backbone in **P1**. Compared with the spectrum of **P1**, the band centered at 831 cm^{-1} (purple-colored), corresponds to *opla* wagging motion of two proximate C–H bonds within the *para*-substituted phenyl rings,[13,22] is absent in that of **8-AGNR**, in line with the annulation of the pendent phenyl rings. A DFT-simulated spectrum of **8-AGNR** agreed well

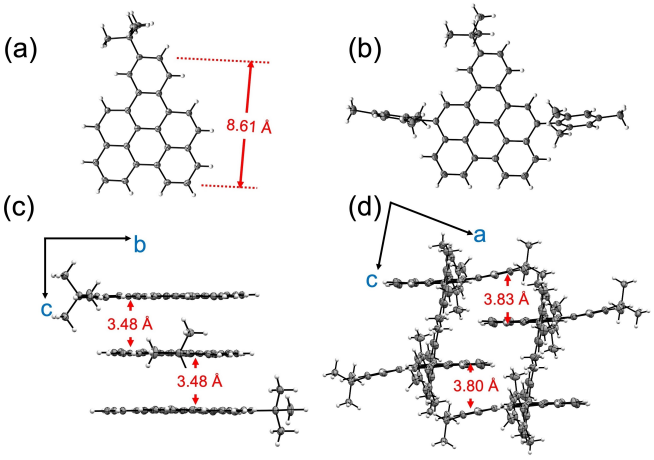

Figure 1. Crystal structures of compounds **1** and **2**. (a, b) ORTEP drawing of **1** and **2**, with thermal ellipsoids shown at 50% probability, respectively. (c, d) Crystal packings of **1** and **2**, respectively.

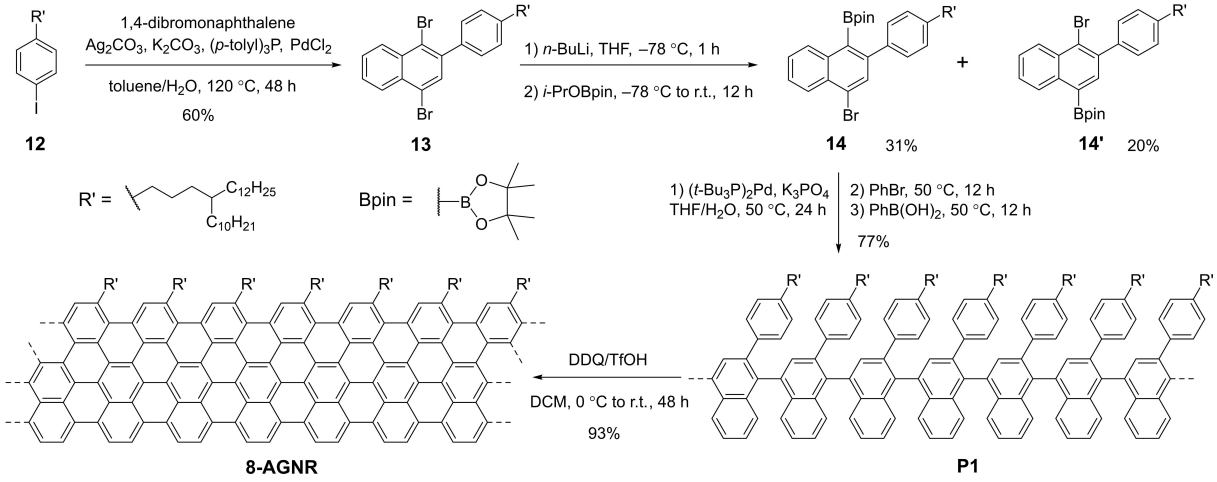

Scheme 2. Schematic illustration of the synthesis of **8-AGNR**.

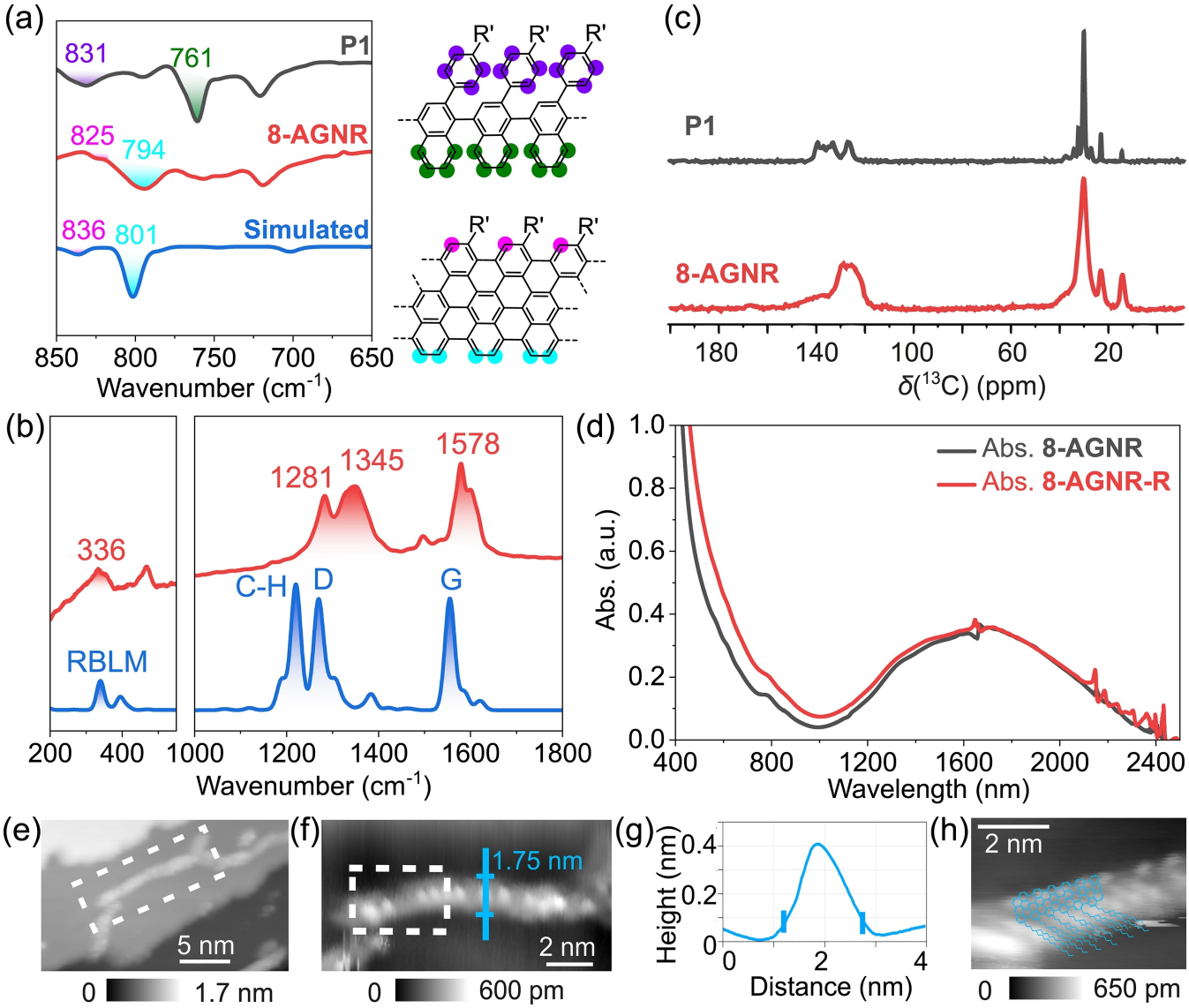

Figure 2. (a) FT-IR spectra of **P1** (black) and **8-AGNR** (red) measured on powder samples and DFT-simulated spectrum of **8-AGNR** (blue). The pink-, cyan-, and olive-colored dots overlaying the chemical structures and the spectra represent SOLO, DUO, and QUATRO vibrational modes of C–H bonds, respectively. The purple-colored dots indicate *opla* C–H wagging motion of neighbouring C–H bonds. (b) Raman spectrum of **8-AGNR** (red) recorded following 532 nm excitations on a powder sample; the blue data corresponds to the simulated Raman spectrum. (c) ^{13}C CP-MAS NMR spectra of **P1** and **8-AGNR** at 700.25 MHz ^{1}H Larmor frequency, 25 kHz MAS, recorded with 3 ms contact time. (d) UV/Vis-NIR spectrum of **8-AGNR** and **8-AGNR-R** (after treatment with hydrazine) in 1,2,4-trichlorobenzene (0.1 mg/mL). (e) STM image of **8-AGNR** on Au(111) at 4.8 K. (f) Zoom-in topography STM image on the dashed rectangle in panel e, displaying the width of a single **8-AGNR**. (g) Height profile along the blue line in panel f. (h) Zoom-in topography STM image on the dashed rectangle region in panel f with an overlayed chemical structure ($I=1$ pA, $U=-300$ mV).

with the experimental result. Two bands observed at 825 cm^{-1} (pink-colored) and 794 cm^{-1} (cyan-colored) could thus be assigned to the SOLO and DUO modes, respectively, corroborating the armchair-edged structure of **8-AGNR**.

The experimental Raman spectrum of **8-AGNR** revealed a notable agreement with the DFT calculation (Figure 2b), enabling us to assign the Raman bands to specific vibrational modes. In general, three peaks of **8-AGNR** centered at 1578, 1345, and 1281 cm^{-1} can be assigned to G, D, and edge C–H peaks, respectively, by comparing with the simulated spectrum (1556, 1270, and 1220 cm^{-1} in the simulated spectrum, respectively, see Supporting Information). The G peak shows a splitting with a shoulder peak at 1598 cm^{-1}, which can be ascribed to the frequency splitting of the longitudinal and transverse optical modes in AGNRs.[23] An absorption peak at the low-energy spectral region is observed at 336 cm^{-1} for **8-AGNR**. This peak is assignable to the radial breathing-like mode (RBLM) according to DFT simulation. Following a zone-folding model,[24] the frequency of RBLM (ω_{RBLM}) is linked to the width of GNR (w_{GNR}) via $\omega_{RBLM}=3222$ Å cm^{-1}/w_{GNR}. The

width of **8-AGNR** is thus estimated to be 0.96 nm, which is fully consistent with the crystallographic results of model compound **1**.

The solid-state ^{1}H magic angle spinning (MAS) and ^{13}C cross-polarization (CP)-MAS NMR characterization of **P1** and **8-AGNR** displayed the broadening of signals, in line with the rigidification of the structures after graphitization (Figures 2c and S12a/b), consistent with previous reports.[2c,25] Moreover, the 2D ^{1}H–^{1}H double quantum-single quantum (DQ-SQ) NMR correlation spectra (Figure S13) are in good agreement with the aimed chemical structure of **P1** and **8-AGNR**. The 2D ^{1}H-^{13}C CP MAS NMR spectrum of **8-AGNR** further demonstrates a close spatial proximity of alkyl chains with delocalized electrons in the core of GNR (see Supporting Information for further details of the solid-state NMR analysis).

Owing to the pendent branched alkyl chains, alleviating the aggregation, **8-AGNR** displays reasonable dispersity in solvents, such as chlorobenzene and 1,2,4-trichlorobenzene (TCB). The absorption of **8-AGNR** dispersed in TCB highlights an extensive red-shift into the NIR region with a broad absorption peak at 1700 nm (Figure 2d). To exclude the contribution of possible oxidized cationic species,[16,26] like radical cations or dications that could be formed under the Scholl reaction, **8-AGNR** was further treated with hydrazine, furnishing a nearly identical spectrum (Figure 2d). Based on the absorption onset, we deduce a record narrow optical band gap of 0.52 eV for **8-AGNR**, close to its theoretically predicted narrow optical band gap of 0.42 eV.[17] This finding further corroborates the successful formation of 8-AGNRs.

High-vacuum electrospray deposition[27] of **8-AGNR** in chlorobenzene on Au(111) enabled us to image its molecular structure by scanning probe microscopy. Assembled structures, presumably consisting of a few **8-AGNR**, were visualized both by STM at 4.8 K (Figure 2e) and non-contact atomic force microscopy (nc-AFM) at room temperature (Figure S16a). The zoom-in topography of a single **8-AGNR** with a length of around 10 nm in Figure 2e shows various white protrusions (Figure 2f), which can be attributed to folded alkyl chains.[28] A width of 1.75 nm is revealed for the isolated **8-AGNR** with a height of 400 pm (Figure 2g). The periodic pattern observed in a close-up topography of a single ribbon is in good agreement with the alkyl chains installed periodically at the edge of **8-AGNR** (Figure 2h). These results provide further structural proof for **8-AGNR**, although higher resolution imaging of **8-AGNR** was impeded by the displacement and distortion of **8-AGNR** on Au(111) surface, even at low temperatures (see Supporting Information).

Optical-pump THz-probe (OPTP) spectroscopy was applied to study the electrical properties of **8-AGNR**. Figure 3a displays the ultrafast complex photoconductivity dynamics of **8-AGNR** dispersed in 1,2,4-trichlorobenzene. A rapid, picosecond rise of photoconductivity ($\triangle\sigma$) is assigned to free carrier generation in GNRs upon photoexcitation (by 3.10 eV laser pulses). Furthermore, the frequency-resolved THz conductivity was recorded 2 ps after the excitation (Figure 3b, see Supporting Information for details). The

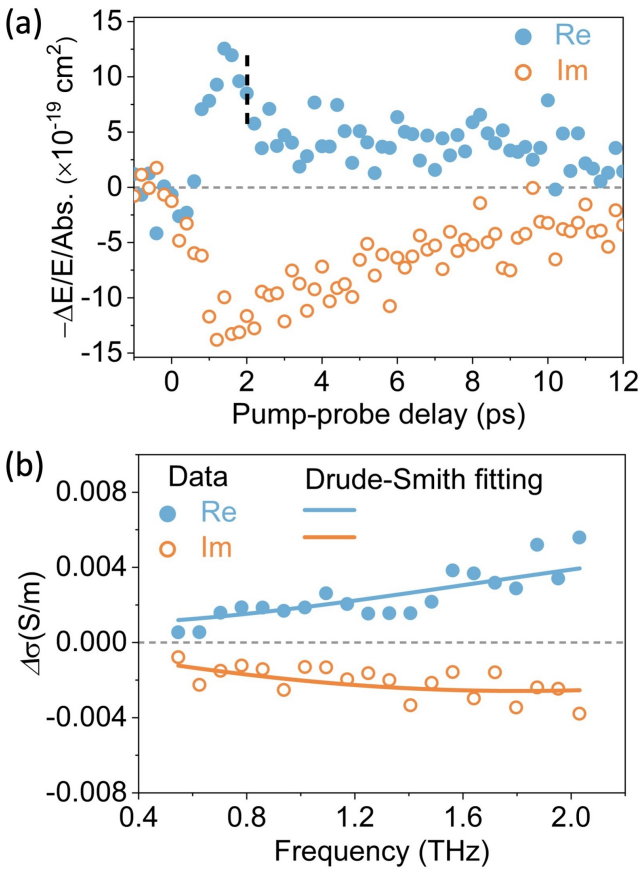

Figure 3. (a) THz photoconductivity dynamics of **8-AGNR** following photoexcitation, normalized to the absorbed photon density. (b) Frequency-resolved THz photoconductivity measured at 2 ps (marked by the dashed vertical line in (a)) after photoexcitation. The solid lines are fits to the Drude–Smith model.

Drude–Smith (DS) model provides an adequate description of the conductivity spectrum. The DS model assumes free charge carriers undergoing preferential backscattering, arising from, e.g., grain boundaries or structural distortions.[2b,29] A parameter c, ranging from 0 (no preferential backscattering, giving the Drude model response) to -1 (complete backscattering), characterizes the backscattering probability. From the fitting, a charge scattering time $\tau = 35 \pm 6$ fs and $c = -0.93 \pm 0.03$ can be derived. A short-range charge mobility in the dc limit of $270 \pm 92\ cm^2\ V^{-1}s^{-1}$ can be inferred following: $\mu_{dc} = \frac{e\tau}{m^*}(1+c)$, $m^* = 0.0163\ m_0$ (see Supporting Information). This value represents a record-high value among the reported GNRs (vs ~20–30 $cm^2\ V^{-1}s^{-1}$ for the previous record in GNRs by the same technique[2c]), which largely originates from the intrinsically small charge carrier effective masses in 8-AGNRs. Finally, the transport properties of **8-AGNR** in a thin film formed by drop-casting were tested (Figure S18). A larger $\tau = 46 \pm 6$ fs and $c = -0.97 \pm 0.03$ are obtained. We thus infer a μ_{dc} of $170 \pm 150\ cm^2\ V^{-1}s^{-1}$ in the film geometry, highlighting the great potential of **8-AGNR** for applications in organic field-effect transistors and photovoltaics, where high mobility is essential for efficient charge transport.

In summary, we demonstrate the first synthesis of 8-AGNRs in solution via an arylated polynaphthalene precursor. Remarkably, the prepared **8-AGNR** exhibit a significant NIR absorption up to 2400 nm and a narrow optical band gap of 0.52 eV. A photoconductivity investigation of **8-AGNR** via THz spectroscopy indicated a high local charge-carrier mobility of ~270 and ~170 $cm^2 V^{-1} s^{-1}$ in dispersion and thin-film of **8-AGNR**, respectively, highlighting this **8-AGNR** as a promising candidate for electronic devices. Furthermore, the novel polymer design strategy developed in this work can facilitate the synthesis of wider AGNRs falling within $N=3p+2$ subgroup, like 11-AGNRs, 14-AGNRs, 17-AGNRs, etc, by simply changing the aryl substituent. Therefore, our study will also open a door for the long-pursued metallic GNRs in solution and further explore their physiochemical properties.

Acknowledgements

This work was financially supported by the Max Planck Society, the FLAG-ERA Grant OPERA by DFG 437130745, and JSPS KAKENHI (Grant Number 21KK0091). X. Yao is grateful for Marie Skłodowska-Curie Research Fellowship (894761-MolecularMAGNET). The authors would like to acknowledge the use of the University of Oxford Advanced Research Computing (ARC) facility. Open Access funding enabled and organized by Projekt DEAL.

Conflict of Interest

The authors declare no conflict of interest.

Data Availability Statement

The data that support the findings of this study are available from the corresponding author upon reasonable request.

Keywords: Carbon Materials · Graphene Nanoribbons · High Charge Carrier Mobility · Low Bandgap · Time-Resolved Spectroscopy

[1] H. Wang, H. S. Wang, C. Ma, L. Chen, C. Jiang, C. Chen, X. Xie, A.-P. Li, X. Wang, *Nat. Rev. Phys.* **2021**, *3*, 791–802.

[2] a) X. Yao, W. Zheng, S. Osella, Z. Qiu, S. Fu, D. Schollmeyer, B. Müller, D. Beljonne, M. Bonn, H. I. Wang, K. Müllen, A. Narita, *J. Am. Chem. Soc.* **2021**, *143*, 5654–5658; b) A. Narita, X. Feng, Y. Hernandez, S. A. Jensen, M. Bonn, H. Yang, I. A. Verzhbitskiy, C. Casiraghi, M. R. Hansen, A. H. R. Koch, G. Fytas, O. Ivasenko, B. Li, K. S. Mali, T. Balandina, S. Mahesh, S. De Feyter, K. Müllen, *Nat. Chem.* **2014**, *6*, 126–132; c) X. Wang, J. Ma, W. Zheng, S. Osella, N. Arisnabarreta, J. Droste, G. Serra, O. Ivasenko, A. Lucotti, D. Beljonne, M. Bonn, X. Liu, M. R. Hansen, M. Tommasini, S. De Feyter, J. Liu, H. I. Wang, X. Feng, *J. Am. Chem. Soc.* **2022**, *144*, 228–235; d) J. Cai, C. A. Pignedoli, L. Talirz, P. Ruffieux, H. Söde, L. Liang, V. Meunier, R. Berger, R. Li, X. Feng, K. Müllen, R. Fasel, *Nat. Nanotechnol.* **2014**, *9*, 896–900; e) D. G. de Oteyza, A. García-Lekue, M. Vilas-Varela, N. Merino-Díez, E. Carbonell-Sanromà, M. Corso, G. Vasseur, C. Rogero, E. Guitián, J. I. Pascual, J. E. Ortega, Y. Wakayama, D. Peña, *ACS Nano* **2016**, *10*, 9000–9008.

[3] a) D. J. Rizzo, G. Veber, T. Cao, C. Bronner, T. Chen, F. Zhao, H. Rodriguez, S. G. Louie, M. F. Crommie, F. R. Fischer, *Nature* **2018**, *560*, 204–208; b) O. Gröning, S. Wang, X. Yao, C. A. Pignedoli, G. Borin Barin, C. Daniels, A. Cupo, V. Meunier, X. Feng, A. Narita, K. Müllen, P. Ruffieux, R. Fasel, *Nature* **2018**, *560*, 209–213.

[4] a) P. Ruffieux, S. Wang, B. Yang, C. Sánchez-Sánchez, J. Liu, T. Dienel, L. Talirz, P. Shinde, C. A. Pignedoli, D. Passerone, T. Dumslaff, X. Feng, K. Müllen, R. Fasel, *Nature* **2016**, *531*, 489–492; b) R. E. Blackwell, F. Zhao, E. Brooks, J. Zhu, I. Piskun, S. Wang, A. Delgado, Y.-L. Lee, S. G. Louie, F. R. Fischer, *Nature* **2021**, *600*, 647–652.

[5] a) J. Liu, P. Ravat, M. Wagner, M. Baumgarten, X. Feng, K. Müllen, *Angew. Chem. Int. Ed.* **2015**, *54*, 12442–12446; b) A. Berdonces-Layunta, J. Lawrence, S. Edalatmanesh, J. Castro-Esteban, T. Wang, M. S. G. Mohammed, L. Colazzo, D. Peña, P. Jelínek, D. G. de Oteyza, *ACS Nano* **2021**, *15*, 5610–5617; c) J. Lawrence, A. Berdonces-Layunta, S. Edalatmanesh, J. Castro-Esteban, T. Wang, A. Jimenez-Martin, B. de la Torre, R. Castrillo-Bodero, P. Angulo-Portugal, M. S. G. Mohammed, A. Matěj, M. Vilas-Varela, F. Schiller, M. Corso, P. Jelinek, D. Peña, D. G. de Oteyza, *Nat. Chem.* **2022**, *14*, 1471–1473.

[6] a) Y.-W. Son, M. L. Cohen, S. G. Louie, *Phys. Rev. Lett.* **2006**, *97*, 216803; b) K. Nakada, M. Fujita, G. Dresselhaus, M. S. Dresselhaus, *Phys. Rev. B* **1996**, *54*, 17954–17961; c) V. Barone, O. Hod, G. E. Scuseria, *Nano Lett.* **2006**, *6*, 2748–2754; d) L. Yang, C.-H. Park, Y.-W. Son, M. L. Cohen, S. G. Louie, *Phys. Rev. Lett.* **2007**, *99*, 186801.

[7] a) G. Li, K.-Y. Yoon, X. Zhong, J. Wang, R. Zhang, J. R. Guest, J. Wen, X. Y. Zhu, G. Dong, *Nat. Commun.* **2018**, *9*, 1687; b) J. Cai, P. Ruffieux, R. Jaafar, M. Bieri, T. Braun, S. Blankenburg, M. Muoth, A. P. Seitsonen, M. Saleh, X. Feng, K. Müllen, R. Fasel, *Nature* **2010**, *466*, 470–473; c) Y.-C. Chen, D. G. de Oteyza, Z. Pedramrazi, C. Chen, F. R. Fischer, M. F. Crommie, *ACS Nano* **2013**, *7*, 6123–6128; d) M. Di Giovannantonio, O. Deniz, J. I. Urgel, R. Widmer, T. Dienel, S. Stolz, C. Sánchez-Sánchez, M. Muntwiler, T. Dumslaff, R. Berger, A. Narita, X. Feng, K. Müllen, P. Ruffieux, R. Fasel, *ACS Nano* **2018**, *12*, 74–81; e) G. Li, K.-Y. Yoon, X. Zhong, X. Zhu, G. Dong, *Chem. Eur. J.* **2016**, *22*, 9116–9120.

[8] a) P. B. Bennett, Z. Pedramrazi, A. Madani, Y.-C. Chen, D. G. de Oteyza, C. Chen, F. R. Fischer, M. F. Crommie, J. Bokor, *Appl. Phys. Lett.* **2013**, *103*, 253114; b) J. P. Llinas, A. Fairbrother, G. Borin Barin, W. Shi, K. Lee, S. Wu, B. Yong Choi, R. Braganza, J. Lear, N. Kau, W. Choi, C. Chen, Z. Pedramrazi, T. Dumslaff, A. Narita, X. Feng, K. Müllen, F. Fischer, A. Zettl, P. Ruffieux, E. Yablonovitch, M. Crommie, R. Fasel, J. Bokor, *Nat. Commun.* **2017**, *8*, 633; c) A. Javey, J. Guo, Q. Wang, M. Lundstrom, H. Dai, *Nature* **2003**, *424*, 654–657; d) T. Dürkop, S. A. Getty, E. Cobas, M. S. Fuhrer, *Nano Lett.* **2004**, *4*, 35–39.

[9] A. Kimouche, M. M. Ervasti, R. Drost, S. Halonen, A. Harju, P. M. Joensuu, J. Sainio, P. Liljeroth, *Nat. Commun.* **2015**, *6*, 10177.

[10] J. Yamaguchi, H. Hayashi, H. Jippo, A. Shiotari, M. Ohtomo, M. Sakakura, N. Hieda, N. Aratani, M. Ohfuchi, Y. Sugimoto, H. Yamada, S. Sato, *Commun. Mater.* **2020**, *1*, 36.

[11] a) K. Sun, P. Ji, J. Zhang, J. Wang, X. Li, X. Xu, H. Zhang, L. Chi, *Small* **2019**, *15*, 1804526; b) H. Huang, D. Wei, J. Sun, S. L. Wong, Y. P. Feng, A. H. C. Neto, A. T. S. Wee, *Sci. Rep.* **2012**, *2*, 983.

[12] X. Xu, A. Kinikar, M. Di Giovannantonio, P. Ruffieux, K. Müllen, R. Fasel, A. Narita, *Bull. Chem. Soc. Jpn.* **2021**, *94*, 997–999.
[13] R. S. Jordan, Y. L. Li, C.-W. Lin, R. D. McCurdy, J. B. Lin, J. L. Brosmer, K. L. Marsh, S. I. Khan, K. N. Houk, R. B. Kaner, Y. Rubin, *J. Am. Chem. Soc.* **2017**, *139*, 15878–15890.
[14] a) A. Narita, Z. Chen, Q. Chen, K. Müllen, *Chem. Sci.* **2019**, *10*, 964–975; b) W. Niu, S. Sopp, A. Lodi, A. Gee, F. Kong, T. Pei, P. Gehring, J. Nägele, C. S. Lau, J. Ma, J. Liu, A. Narita, J. Mol, M. Burghard, K. Müllen, Y. Mai, X. Feng, L. Bogani, *Nat. Mater.* **2023**, *22*, 180–185.
[15] W. Yang, A. Lucotti, M. Tommasini, W. A. Chalifoux, *J. Am. Chem. Soc.* **2016**, *138*, 9137–9144.
[16] D. Jänsch, I. Ivanov, Y. Zagranyarski, I. Duznovic, M. Baumgarten, D. Turchinovich, C. Li, M. Bonn, K. Müllen, *Chem. Eur. J.* **2017**, *23*, 4870–4875.
[17] D. Prezzi, D. Varsano, A. Ruini, A. Marini, E. Molinari, *Phys. Rev. B* **2008**, *77*, 041404.
[18] B. T. King, J. Kroulík, C. R. Robertson, P. Rempala, C. L. Hilton, J. D. Korinek, L. M. Gortari, *J. Org. Chem.* **2007**, *72*, 2279–2288.
[19] Deposition numbers 2243983 (for **1**) and 2243984 (for **2**) contain the supplementary crystallographic data for this paper. These data are provided free of charge by the joint Cambridge Crystallographic Data Centre and Fachinformationszentrum Karlsruhe Access Structures service.
[20] K.-H. Liu, G.-Q. Hu, C.-X. Wang, F.-F. Sheng, J.-W. Bai, J.-G. Gu, H.-H. Zhang, *Org. Lett.* **2021**, *23*, 5626–5630.
[21] M. Tommasini, A. Lucotti, M. Alfè, A. Ciajolo, G. Zerbi, *Spectrochim. Acta Part A* **2016**, *152*, 134–148.
[22] N. B. Colthup, L. H. Daly, S. E. Wiberley, *Introduction to infrared and Raman spectroscopy, 3rd ed*, Academic Press, San Diego, CA, **1990**.
[23] R. Gillen, M. Mohr, C. Thomsen, J. Maultzsch, *Phys. Rev. B* **2009**, *80*, 155418.
[24] R. Gillen, M. Mohr, J. Maultzsch, *Phys. Rev. B* **2010**, *81*, 205426.
[25] a) M. M. Elmahdy, X. Dou, M. Mondeshki, G. Floudas, H.-J. Butt, H. W. Spiess, K. Müllen, *J. Am. Chem. Soc.* **2008**, *130*, 5311–5319; b) W. Niu, Y. Fu, G. Serra, K. Liu, J. Droste, Y. Lee, Z. Ling, F. Xu, J. D. Cojal González, A. Lucotti, J. P. Rabe, M. Ryan Hansen, W. Pisula, P. W. M. Blom, C.-A. Palma, M. Tommasini, Y. Mai, J. Ma, X. Feng, *Angew. Chem. Int. Ed.* **2023**, *62*, e202305737.
[26] A. Matsumoto, M. Suzuki, D. Kuzuhara, H. Hayashi, N. Aratani, H. Yamada, *Angew. Chem. Int. Ed.* **2015**, *54*, 8175–8178.
[27] a) S. Scherb, A. Hinaut, X. Yao, A. Götz, S. H. Al-Hilfi, X.-Y. Wang, Y. Hu, Z. Qiu, Y. Song, K. Müllen, T. Glatzel, A. Narita, E. Meyer, *ACS Nano* **2023**, *17*, 597–605; b) A. Hinaut, S. Scherb, S. Freund, Z. Liu, T. Glatzel, E. Meyer, *Beilstein J. Nanotechnol.* **2021**, *12*, 552–558.
[28] O. Endo, M. Nakamura, K. Amemiya, H. Ozaki, *Langmuir* **2017**, *33*, 3934–3940.
[29] I. Ivanov, Y. Hu, S. Osella, U. Beser, H. I. Wang, D. Beljonne, A. Narita, K. Müllen, D. Turchinovich, M. Bonn, *J. Am. Chem. Soc.* **2017**, *139*, 7982–7988.

Manuscript received: August 27, 2023
Accepted manuscript online: September 26, 2023
Version of record online: October 10, 2023